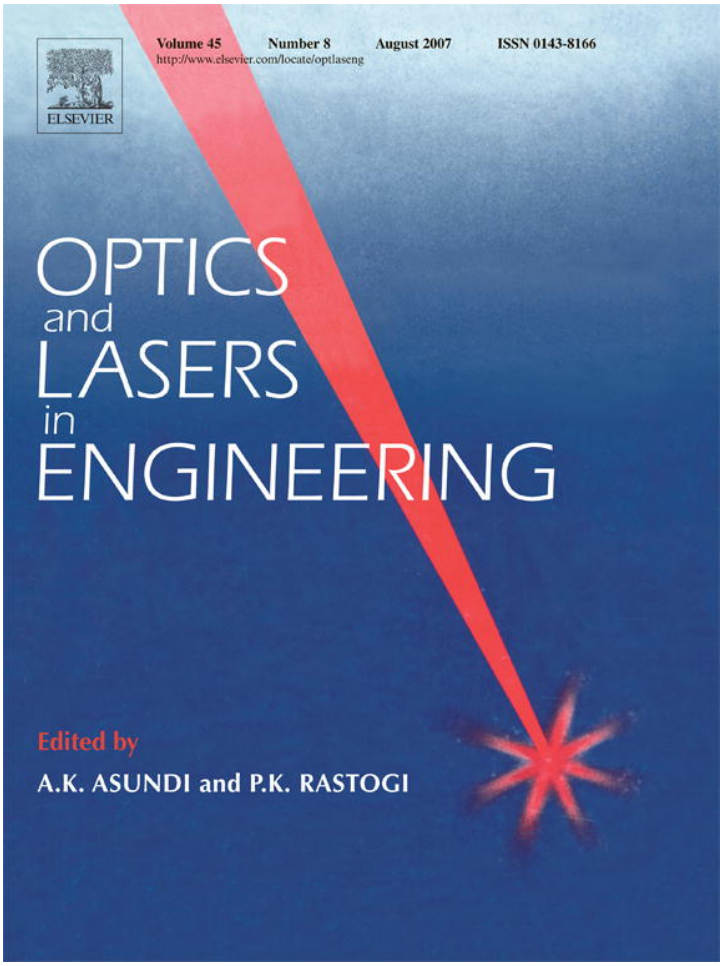

Available online at www.sciencedirect.com
ScienceDirect
Optics and Lasers in Engineering 45 (2007) 868–876
OPTICS and LASERS in ENGINEERING
www.elsevier.com/locate/optlaseng

Reducing phase retrieval errors in Fourier analysis of 2-dimensional digital model interferograms

Jadranko Gladić*, Zlatko Vučić, Davorin Lovrić

Institute of Physics, Bijenička cesta 46, P. O. Box 304, 10001 Zagreb, Croatia

Received 22 November 2006; received in revised form 19 December 2006; accepted 31 January 2007
Available online 26 March 2007

Abstract

In order to measure the displacements of facets on a growing spherical $Cu_{2-\delta}Se$ crystal with sub-nanometre resolution, we investigated the reliability and accuracy of standard method of Fourier analysis of digital laser interferograms. Guided by realistic experimental conditions (two-dimensional (2D) interferograms), starting from 2D model interferograms and using original custom designed Gaussian filtering window and multistage unwrapping procedure of the retrieved phase, we demonstrate for a considerable parameter range the non-negligible inherent phase retrieval error due to non-integer number of fringes within the digital image. Our results indicate an intermediate parameter range where the error is acceptably small. We introduce an algorithm modification that significantly reduces the error, especially for low and high fringe densities. In the experimentally most common case of diagonal fringes the reduced error is an order of magnitude smaller than for nearly one-dimensional case within almost entire parameter space.

Keywords: Digital image processing; Fringe analysis; Phase retrieval; Crystal growth

1. Introduction

Investigations by Ohachi's group [1–3] and our investigations [4–6] of superionic conductors, copper and silver chalcogenides, materials with high diffusivity of Cu and Ag atoms, enabled their promotion as new members of rather small group of materials that form equilibrium crystal shape (ECS), being the only ones that besides ^{4}He form ECS of macroscopic size (spherical faceted crystals of several millimetres in diameter). The size is crucial for investigating the non-equilibrium processes, i.e. shape kinetics during crystal growth as a function of the supersaturation forces driving the growth. Apart from thermodynamic reasons (approaching the limit of infinite size crystal), the macroscopic size is especially important in the case of crystals growing at high temperatures at which the STM and AFM techniques are not applicable. Using two-beam optical interferometry (at growth velocities from 0.01 nm/s to a few tens of nm/s, with declared resolution well below 10 nm) and by monitoring pressure of the liquid as a level gauge (0.05–50 μm/s) for investigating growth of ^{4}He crystals at 2–250 mK, new facet growth modes were detected [7] the mechanism of which is not quite understood. On the other hand, our preliminary studies show that copper selenide ECS crystals at around 800 K exhibit similar facet growth modes. For their modelling, the temperature complementarity of ^{4}He and superionic conductors crystals seems to be of essential importance.

Our goal is to measure as precisely as possible the values of geometrical parameters of facets and curved parts of growing crystal surface necessary for characterizing the growth kinetics of our spherical single crystals in order to understand better the observed modes of growth. Using the facets as highly reflecting objects, we apply digital laser interferometry method with refined [8] Fourier transform method of fringe pattern analysis to measure the displacements of facet perpendicular to the facet plane with sub-nanometre resolution.

In order to test the reliability and accuracy of the standard procedure of phase retrieval from the interference fringe pattern [7–10] by using the usual fringe Fourier

*Corresponding author. Tel.: +38514698809; fax: +38514698889.
E-mail address: gladic@ifs.hr (J. Gladić).

0143-8166/$ - see front matter © 2007 Elsevier Ltd. All rights reserved.
doi:10.1016/j.optlaseng.2007.01.006

analysis method, we have started [11] by testing the method itself applying it to an artificial, idealized fringe pattern in simple case where the 2-dimensional (2D) fringe pattern is reduced to its 1-dimensional (1D) projection (where the x-axis is set to be perpendicular to the interferometric fringes). The method used as described in work of Kostianovski et al. [9] revealed the error in retrieved phase compared to the initially imposed phase in the model pattern. This inherent error was shown to originate from the non-integer number of fringes in the discrete image field, and its dependence on spatial carrier frequency, initial phase value and the deviation of number of fringes from integer value was investigated. We suggested a modification of the usual algorithm which proved to reduce the retrieved phase error more than threefold.

Under the usual experimental conditions it is extremely rare that the fringe pattern is obtained which can be treated within the 1D formalism. Therefore, we outline here the modifications necessary for treatment of realistic general 2D case, introducing the original design of the Gaussian filtering window (appropriate for 2D case) and giving explicit formulas for phase retrieval in the real-life experimental situation which are shown to reduce the inherent phase determination errors particularly for low and high densities of fringes. The error magnitude dependence on the parameters of experimentally obtained interferometric fringe patterns is clearly demonstrated. It turns out that in the case of diagonally running fringes within 2D image field not only is the inherent error smaller, but also our algorithm reduces it to the level that is an order of magnitude lower than for 1D projection within almost the entire parameter space.

2. Fringe-pattern Fourier analysis

2.1. Interferometric images

During the crystal growth experiment we acquire, as a rule, a large number of 2D fringe patterns using a CCD camera. It takes frames at regular time intervals (25 frames/s) of the part of growing crystal surface including the facet with interference fringes. The background noise is automatically reduced by two orders of magnitude by applying an original algorithm [8], the area with fringe pattern corresponding to the facet is detected and a small square part of 64×64 pixels is extracted for further analysis, particularly for retrieval of the phase field value.

As we are actually dealing with the CCD camera digitized image, we stress that the fringe pattern intensity field $i(\vec{r})$ is a 2D set of $N \times M$ discrete intensities recorded separately as pixels with 6–12 bit intensity resolution (depending on the CCD camera and frame grabber used).

In the general case of non-quadratic pixels, $x = nd_{\mathrm{p}}^{x}$, $y = md_{\mathrm{p}}^{y}$ where d_{p}^{x} and d_{p}^{y} are pixel dimensions, and n and m are number of pixels in the x and y directions ($-N/2 \leqslant n \leqslant N/2-1$, $-M/2 \leqslant m \leqslant M/2-1$), respectively.

The fringe pattern intensity is described by

$$i(x,y) = a(x,y) + 2b(x,y)\cos[(Q_x x + Q_y y + \varphi(x,y)], \qquad (1)$$

$$Q_x = \frac{2\pi}{Nd_{\mathrm{p}}^{x}}(k_Q^x + D_Q^x), \quad Q_y = \frac{2\pi}{Md_{\mathrm{p}}^{y}}(k_Q^y + D_Q^y),$$

$$0 \leqslant k_Q^x \leqslant \frac{N}{2} - 1, \quad -\frac{M}{2} \leqslant k_Q^y \leqslant \frac{M}{2} - 1,$$
$$-0.5 < D_Q^x \leqslant 0.5, \quad -0.5 < D_Q^y \leqslant 0.5,$$

$$\varphi(x,y) = 2\pi\phi(x,y),$$

with the origin in the centre of the image field.

The modulation wave vector $\vec{Q}$ (spatial carrier frequency) is expressed as the sum of an integer ($\vec{k}_Q$) and a non-integer ($\vec{D}_Q$) component in units of discrete Fourier space. The integers k_Q^x and k_Q^y are fixed during the entire experiment (determined by fine adjusting the experimental set-up), while the non-integer components oscillate in time from one image to the next one [8]. For the application of procedure described in this article, the modulation wave vector is determined for every image (in particular its non-integer component, e.g. by use of sampling theorem [8]).

As suggested by Takeda et al. [10] the spatial frequency spectrum of the interferograms is obtained by writing Eq. (1) in the complex form and by doing the discrete Fourier transformation in 2 dimensions (k^x, k^y Fourier space; $-N/2 \leqslant k^x \leqslant N/2-1$, $-M/2 \leqslant k^y \leqslant M/2-1$).

In order to proceed with an exact calculation we make an approximation by choosing that the magnitude of the background intensity a, the amplitude of the modulation b, and the phase ϕ are slowly varying quantities within the image frame and can be represented by their average values over the fringe pattern field: $a(n,m) = \bar{a}$, $b(n,m) = \bar{b}$, $\phi(n,m) = \bar{\phi}$. (This approximation is quite realistic bearing in mind that in the experiments we are using small (typically 64×64) image sub-frames, extracted from much larger original CCD camera frame after reducing the background noise by two orders of magnitude.)

We obtain three separate terms, corresponding to the negative first-order maximum, central maximum and the positive first-order maximum, respectively.

Following the usual procedure, in order to retrieve the phase of the interference pattern, we now shift the Fourier spectrum in such a way that one of the side maxima is moved to the position $\vec{k} = 0$, thus removing the carrier frequency.

As we are dealing with discrete signal (intensities of pixels), the shift of the spectrum can unfortunately be done exclusively by an integer number $\vec{k}_Q$. By formally replacing $k^x \to k^x + k_Q^x$, $k^y \to k^y + k_Q^y$, we obtain

$$\bar{C}^{\mathrm{appr.}}(k^x,k^y) = \frac{\bar{b}}{NM}\exp\left[-\mathrm{j}2\pi\left(\bar{\phi} - \frac{D_Q^x}{2N} - \frac{D_Q^y}{2M}\right)\right]$$

$$\times \exp\left[\mathrm{j}\pi\left(\frac{k^x+2k_Q^x}{N}+\frac{k^y+2k_Q^y}{M}\right)\right]$$
$$\times \mathrm{SINC}(k^x+2k_Q^x+D_Q^x)$$
$$\times \mathrm{SINC}(k^y+2k_Q^y+D_Q^y)$$
$$+\frac{\bar{a}}{NM}\exp\left[\mathrm{j}\pi\left(\frac{k^x+k_Q^x}{N}+\frac{k^y+k_Q^y}{M}\right)\right]$$
$$\times \mathrm{SINC}(k^x+k_Q^x)\mathrm{SINC}(k^y+k_Q^y)$$
$$+\frac{\bar{b}}{NM}\exp\left[\mathrm{j}2\pi\left(\bar{\phi}-\frac{D_Q^x}{2N}-\frac{D_Q^y}{2M}\right)\right]$$
$$\times \exp\left[\mathrm{j}\pi\left(\frac{k^x}{N}+\frac{k^y}{M}\right)\right]\mathrm{SINC}(k^x-D_Q^x)$$
$$\times \mathrm{SINC}(k^y-D_Q^y), \quad (2)$$

where $\bar{C}^{\mathrm{appr.}}(k^x,k^y)$ denotes the shifted FFT spectrum of the 2D fringe pattern. The first of the three terms in this sum is the former negative first-order maximum, the second one is the former central maximum, and the third is the former positive first-order maximum, all shifted by the $(-k_Q^x,-k_Q^y)$ vector. The positive first-order maximum thus comes to the position very near the origin, being left off-centre for the non-integral (D_Q^x,D_Q^y).

All three terms contain similar finite geometrical series of the type

$$\sum_{l=-L/2}^{L/2-1}\exp\left(-\mathrm{j}\frac{2\pi}{L}pl\right)=\exp\left(\mathrm{j}\frac{\pi}{L}p\right)\mathrm{SINC}(p),$$
$$\mathrm{SINC}(p)=\frac{\sin(\pi p)}{\sin((\pi/L)p)}, \quad (3)$$

for $L=N$, M and $l=n$, m.

The SINC functions as defined in Eq. (3) are for $\vec{D}_Q\neq 0$ spread over the reciprocal space and their intensities are also significant in regions far from their corresponding maximum, even in the position of the respective maximum of the opposite sign (they are the source of intensity leakage to nearby spatial frequencies).

The intensities in the Fourier space are strongly influenced by the behaviour of the SINC functions, dependent on the non-integer part of the number of fringes contained within the field of pixels in both directions (D_Q^x, D_Q^y). When the number of fringes is exactly an integer ($\vec{D}_Q=0$), there is no intensity leakage to spectral frequencies outside the well defined three maxima, and the spectrum is equal to zero everywhere except at the positions $\vec{k}=-2\vec{k}_Q$, $\vec{k}=-\vec{k}_Q$, and $\vec{k}=0$. For a non-integer number of fringes ($\vec{D}_Q\neq 0$) each of the terms representing the first (positive and negative) maxima is spread out over the entire Fourier space (visible "ridges" in Fig. 1, showing the situation before shifting the Fourier spectrum). Thus the two complex conjugated first order maxima overlap at each point of the reciprocal space, the strength of overlapping being proportional to the size of $\vec{D}_Q$. There is also a significant intensity cutoff at the Nyquist frequency for $\vec{D}_Q\neq 0$.

2.2. Filtering using the 2D Gaussian window

In order to extract the phase information from the spectrum, the standard procedure is to isolate the shifted former first positive maximum from the rest of the spectrum. This is done by filtering of the Fourier spectrum by a narrow rectangular window centred at the origin ($\vec{k}=0$) and apodized by a suitable Gaussian function, as suggested before [7,9]. It should accommodate to any particular experimentally obtained density of fringes, having at the same time minimal possible influence on the spatial resolution. Our custom designed filtering function is centred at the origin of reciprocal space, including the concept of the adjustable width depending on separation of first-order maxima and the positions of edges of the Fourier space. Its role is to reduce the intensity of the former central maximum (now shifted to $-\vec{k}_Q$) as well as the former first negative maximum (now shifted to $-2\vec{k}_Q$). It is also used to remove the intensity jumps formerly located at the Nyquist frequencies (the edges of the field now at $N/2-1-|k_Q^x|$ and $M/2-1-|k_Q^y|$).

The Gaussian window of the following form fulfils all the mentioned requirements:

$$\mathrm{GW}_{2\mathrm{D}}=\exp\left\{-\alpha\ln 10\frac{((N/2)-2)^2((M/2)-1)^2}{[(k_Q^x)^2+(k_Q^y)^2]((N/2)-1-|k_Q^x|)^2((M/2)-1-|k_Q^y|)^2}k^2\right\}. \quad (4)$$

The factor α determines the level to which the former central maximum is reduced in intensity, i.e., it is multiplied by a factor $10^{-\alpha}$ ($\alpha\geqslant 3$) and suppressed at least to a level comparable with noise. (The results weakly depend on the value of α).

2.3. Inverse fast Fourier transformation and phase extraction

By denoting $\psi=\bar{\phi}-D_Q^x/2N-D_Q^y/2M$ we now have

$$\bar{C}_{\mathrm{W}}^{\mathrm{appr.}}(k^x,k^y)=\frac{\bar{b}}{NM}\left\{\begin{array}{l}\exp(-\mathrm{j}2\pi\psi)\exp\left[\mathrm{j}\pi\left(\frac{k^x+2k_Q^x}{N}+\frac{k^y+2k_Q^y}{M}\right)\right]\\ \times\mathrm{SINC}(k^x+2k_Q^x+D_Q^x)\mathrm{SINC}(k^y+2k_Q^y\\ +D_Q^y)\mathrm{GW}_{2\mathrm{D}}+\exp(\mathrm{j}2\pi\psi)\exp\left[\mathrm{j}\pi\left(\frac{k^x}{N}+\frac{k^y}{M}\right)\right]\\ \times\mathrm{SINC}(k^x-D_Q^x)\mathrm{SINC}(k^y-D_Q^y)\mathrm{GW}_{2\mathrm{D}}\end{array}\right\}$$
$$+\mathrm{occ(FCM)}. \quad (5)$$

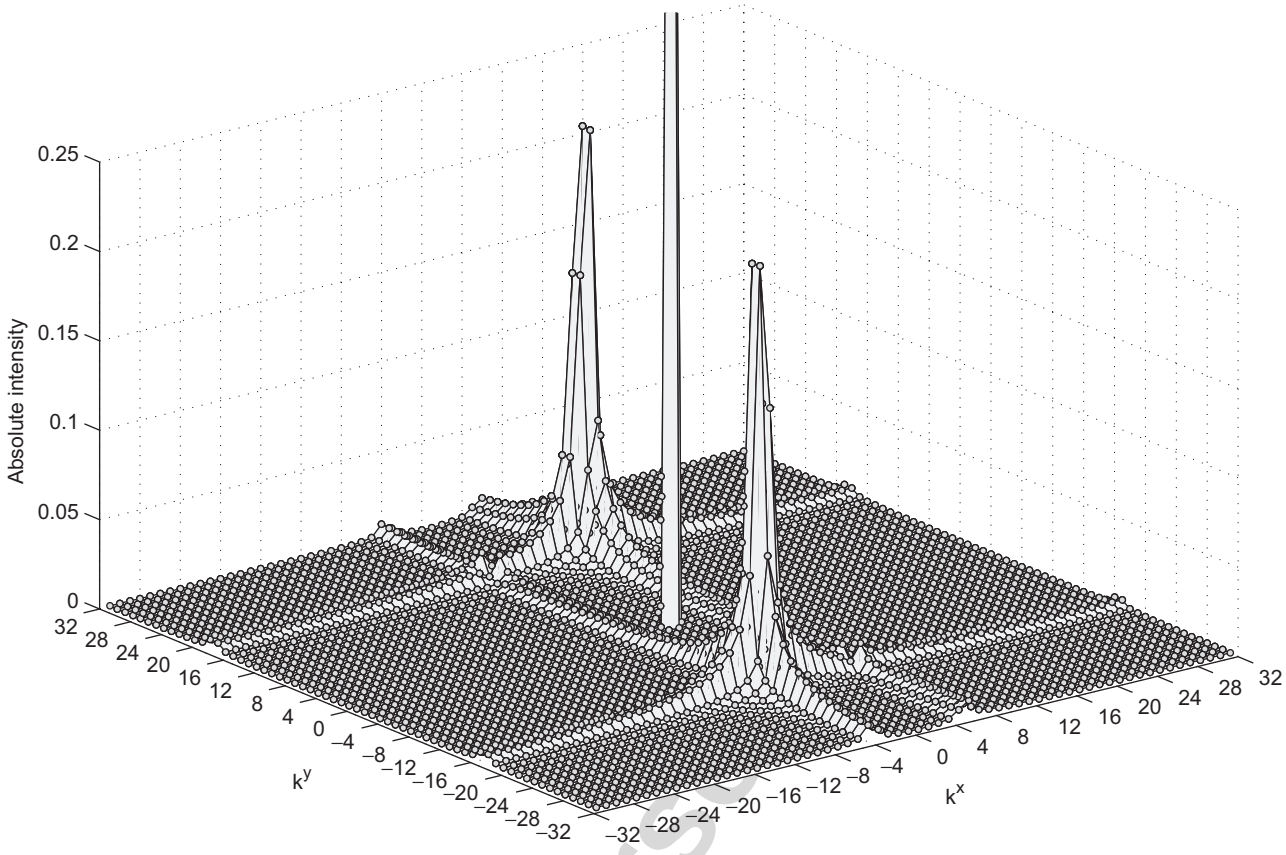

Fig. 1. The leakage effect originating from the SINC functions in the Fourier spectrum with shown narrow central maximum and positive and negative first-order maxima (enlarged). Parameters are: $N = M = 64$, $\bar{b}/\bar{a} = 0.5$, $\phi = 0.155$, $k_Q^x = 5$, $k_Q^y = 17$, $D_Q^x = 0.5$ and $D_Q^y = 0.5$.

The former central maximum is after applying the filter function (Gaussian window) reduced in amplitude over 1000 times, and is therefore denoted as occ(FCM) and neglected in further calculations.

The influence of the leakage effect (Fig. 1) is still clearly visible through the presence of SINC functions in Eq. (5), originating, as already stressed, as a direct consequence of $\vec{D}_Q \neq 0$, which cannot be removed by the application of Gaussian window filter (or any other window function [12] for that matter), no matter how efficient and narrow it would be.

Following the standard recipe, the next step would be the application of the inverse Fourier transform to the shifted and filtered spectrum $\bar{C}_{\mathrm{W}}^{\mathrm{appr.}}(k^x, k^y)$, to obtain a complex function $I(n,m)$ in the real space from which the phase would be extracted. The following ubiquitous formula for extracting the phase field from the inverse Fourier transform is not accurate enough:

$$\bar{\phi} = \frac{D_Q^x}{2N} + \frac{D_Q^y}{2M} + \frac{1}{2\pi}\arctan\left\{\frac{\mathrm{Im}[I(n,m)]}{\mathrm{Re}[I(n,m)]}\right\}, \tag{6}$$

$$I(n,m) = \mathrm{IFFT}\left[\bar{C}_{\mathrm{W}}^{\mathrm{appr.}}(k^x, k^y)\right] = \frac{1}{NM}\sum_{k^x=-N/2}^{N/2-1}\sum_{k^y=-M/2}^{M/2-1}\bar{C}_{\mathrm{W}}^{\mathrm{appr.}}(k^x, k^y) - 2pt\times\exp\left[\mathrm{j}2\pi\left(\frac{k^x n}{N} + \frac{k^y m}{M}\right)\right]. \tag{7}$$

Note that there is also the linear phase correction, $D_Q^x/2N + D_Q^y/2M$, independent of carrier frequency, inversely proportional to the dimensions of the image field $N \times M$.

3. Results and discussion

The main disadvantage of the method is the x–y resolution problem originating from the artificial retrieved phase field modulation introduced inevitably from the incomplete shift (by the integer valued vector) of the first positive maximum towards the origin, thus being left off centre by $\vec{D}_Q$. In order to determine the retrieved phase error as compared with the initially introduced phase, we are forced to do the averaging over the entire retrieved phase field.

In the real experimental data the non-integer $\vec{D}_Q$ changes from one image to the next [8], so that its influences on the retrieved phase field modulation do not cancel out when calculating the changes in the phase field between consecutive images. Therefore, it is not possible to obtain the reconstruction of fine details of the growing crystal facet–the only reliable information one can get is about the

change of position of the growing facet calculated from averaged phase field over the entire $N \times M$ (typically 64×64 pixels) selected fringe pattern area. Taking these regions from different parts of the facet image can give some local information about the surface profile changes, the $x-y$ resolution being given by the size of the crystal surface corresponding to the selected region (depending on the magnification of the experimental set-up).

Before averaging, because of these same artificial modulations, the appropriate 2D unwrapping must be applied. Fortunately, the simple methods found in standard mathematical software prove to be quite appropriate (but should be applied with care, consecutively first to columns, then to rows of the matrix), except in a few rare occasions where the previous application of an "initial preparatory" unwrapping following the algorithm by Abbas [13] helps to remove some problematic phase jumps.

The dependence of the retrieved phase error (using standard Eq. (6)) on integer part components of the spatial carrier frequency k_Q^x and k_Q^y is shown in Fig. 2 (for the input phase $\phi_{\text{in}} = 0.155$ that produces maximum error, and for the most unfavourable case of the maximum possible departure from the integer values $D_Q^x = 0.5$ and $D_Q^y = 0.5$).

Dependence of the averaged retrieved phase error value (using standard Eq. (6)) on non-integer part of the spatial carrier frequency $\vec{D}_Q = (D_Q^x,\ D_Q^y)$ is shown by larger circles in Fig. 3., within a small part of the Fourier space. The error vanishes for $\vec{D}_Q = 0$, and is starting to show up with departure from the integer value of the carrier frequency, diminishing as the k_Q^y component grows.

4. Corrected phase extraction

By introducing $\bar{C}_{\text{W}}^{\text{appr.}}(k^x, k^y)$ from Eq. (5) into the expression (7) for $I(n,m)$ and omitting the occ(FCM) term, we have

Sums in both terms are recognized as the inverse Fourier transforms of mutually similar functions which we denote K and O, hereby explicitly listed by components ($i = x,\ y$, $L = N,\ M$, respectively):

$$K^i(k^i) = \exp\left(\mathrm{j}\pi\frac{k^i + 2k_Q^i}{L}\right)\mathrm{SINC}(k^i + 2k_Q^i + D_Q^i)\mathrm{GW}_{2\mathrm{D}}^i,$$

$$O^i(k^i) = \exp\left(\mathrm{j}\pi\frac{k^i}{L}\right)\mathrm{SINC}(k^i - D_Q^i)\mathrm{GW}_{2\mathrm{D}}^i. \tag{9}$$

Using this notation we have

$$I(n,m) = \frac{\bar{b}}{N^2M^2}\left\{\begin{array}{c}\exp(-\mathrm{j}2\pi\psi)\mathrm{IFFT}\ K^x(n)\mathrm{IFFT}\ K^y(m) + \\ +\exp(\mathrm{j}2\pi\psi)\mathrm{IFFT}\ O^x(n)\mathrm{IFFT}\ O^y(m)\end{array}\right\}. \tag{10}$$

It can be shown that $K = K^xK^y$ and $O = O^xO^y$ ($\mathrm{GW}_{2\mathrm{D}} = \mathrm{GW}_{2\mathrm{D}}^x\mathrm{GW}_{2\mathrm{D}}^y$). Solving this equation as a linear system of equations for the sine and the cosine of the corrected phase $\psi = \bar{\phi} - D_Q^x/2N - D_Q^y/2M$, by using the real and imaginary parts of these functions, we finally obtain a somewhat complicated, but more accurate expression for phase retrieval:

$$\tan 2\pi\psi = \frac{\mathrm{Im}\{[\mathrm{IFFT}(O+K)]^*\tilde{I}\}}{\mathrm{Re}\{[\mathrm{IFFT}(O-K)]^*\tilde{I}\}}, \tag{11}$$

$$\bar{\phi} = \frac{D_Q^x}{2N} + \frac{D_Q^y}{2M} + \frac{1}{2\pi}\arctan\left\{\frac{\mathrm{Im}\{[IFFT(O+K)]^*\tilde{I}\}}{\mathrm{Re}\{[IFFT(O-K)]^*\tilde{I}\}}\right\}, \tag{12}$$

where $\tilde{I} = (N^2M^2/\bar{b})I(n,m)$.

(Just like in the case of using Eq. (6), the appropriate 2D unwrapping must be applied to the retrieved phase, followed by averaging over the entire phase field.) This introduces some more computational effort as compared to the standard (less accurate) expression (6), but the improvement is obvious from Fig. 3, where the phase values obtained from this expressions are shown with smaller grey circles. The error amplitude is significantly

$$I(n,m) = \frac{\bar{b}}{N^2M^2}\left\{\begin{array}{l}\exp(-\mathrm{j}2\pi\psi)\sum\limits_{k^x=-N/2}^{N/2-1}\exp\left(\mathrm{j}2\pi\frac{k^xn}{N}\right)\exp\left(\mathrm{j}\pi\frac{k^x+2k_Q^x}{N}\right) \\ \times\mathrm{SINC}(k^x + 2k_Q^x + D_Q^x)\sum\limits_{k^y=-M/2}^{M/2-1}\exp\left(\mathrm{j}2\pi\frac{k^ym}{M}\right)\exp\left(\mathrm{j}\pi\frac{k^y+2k_Q^y}{M}\right) \\ \times\mathrm{SINC}(k^y + 2k_Q^y + D_Q^y)\mathrm{GW}_{2\mathrm{D}} + \exp(\mathrm{j}2\pi\psi) \\ \times\sum\limits_{k^x=-N/2}^{N/2-1}\exp\left(\mathrm{j}2\pi\frac{k^xn}{N}\right)\exp\left(\mathrm{j}\pi\frac{k^x}{N}\right)\mathrm{SINC}(k^x - D_Q^x) \\ \times\sum\limits_{k^y=-M/2}^{M/2-1}\exp\left(\mathrm{j}2\pi\frac{k^ym}{M}\right)\exp\left(\mathrm{j}\pi\frac{k^y}{M}\right)\mathrm{SINC}(k^y - D_Q^y)\mathrm{GW}_{2\mathrm{D}}\end{array}\right\}. \tag{8}$$

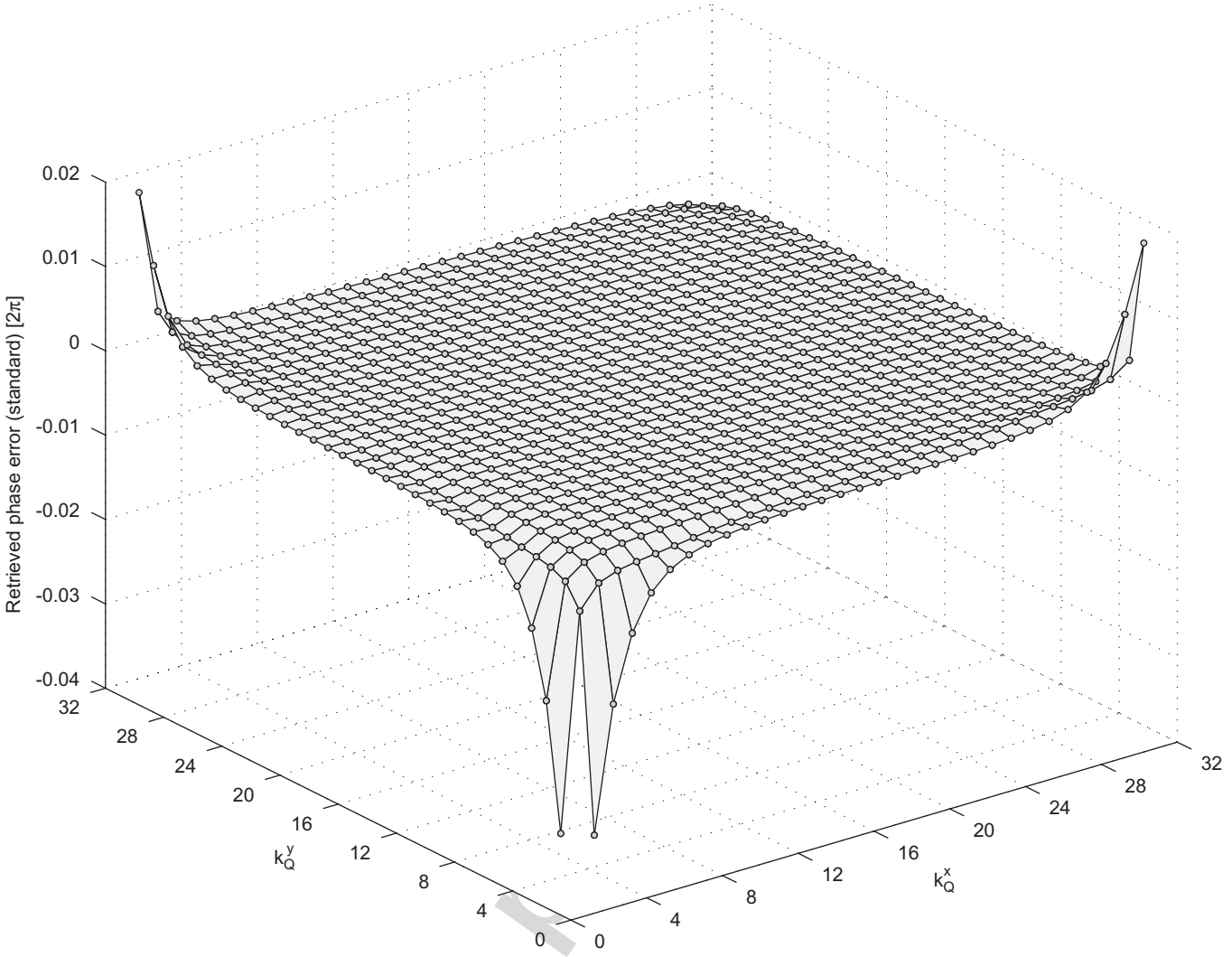

Fig. 2. Difference between the retrieved phase (from Eq. (6)) and the initially set phase, in units of 2π, as a function of integer spatial frequency components k_Q^x and k_Q^y. Parameters are: $N = M = 64$, $\bar{b}/\bar{a} = 0.5$, $\phi_{in} = 0.155$, $\alpha = 3$, $D_Q^x = 0.5$ and $D_Q^y = 0.5$.

reduced. It can be further suppressed by increasing the value of α in the Gaussian window definition (taking care that it still makes sense, concerning the noise present in realistic experiments – the removal of noise from original data [8] is an obligatory prerequisite for high-quality measurements).

In analogy with Fig. 2, the dependence of the retrieved phase error using this corrected expression given by Eq. (12) on integer part components of the spatial carrier frequency k_Q^x and k_Q^y is shown in Fig. 4 (again for the most unfavourable case of $\phi_{in} = 0.155$, and $D_Q^x = 0.5$, $D_Q^y = 0.5$).

In order to emphasize the significance of the improved (corrected) expression for phase retrieval and to demonstrate its beneficial effect in real experimental situations, we show in Fig. 5. two cross-sections of combined Figs. 2 and 4. In the upper part we show the behaviour of retrieved phase error in the case of interferometric fringes exactly parallel to the image x-axis ($k_Q^y = 0$), while in the lower part we show the error in the case of fringes running diagonally over the image field ($k_Q^x = k_Q^y$). The error of the retrieved phase (averaged over the whole field) is shown in nanometres. (It is in fact the error in determination of the displacement $\Delta\bar{z}$ of the growing facet in the direction perpendicular to its plane obtained by using the formula

$$\Delta\bar{z} = \Delta\bar{\phi}\frac{\lambda}{4\pi\cos(\theta/2)}, \tag{13}$$

where $\Delta\bar{\phi}$ is the difference between values of the averaged unwrapped retrieved phase field from two consecutive interferograms, $\lambda = 632.8$ nm for He–Ne laser, and the angle between the incident and the reflected beam $\theta = 0^\circ$). Diamonds show the error obtained using the standard Eq. (6), and squares the corrected value according to Eq. (12). The error itself is obviously smaller for fringes running diagonally (due to the fact that in this case the

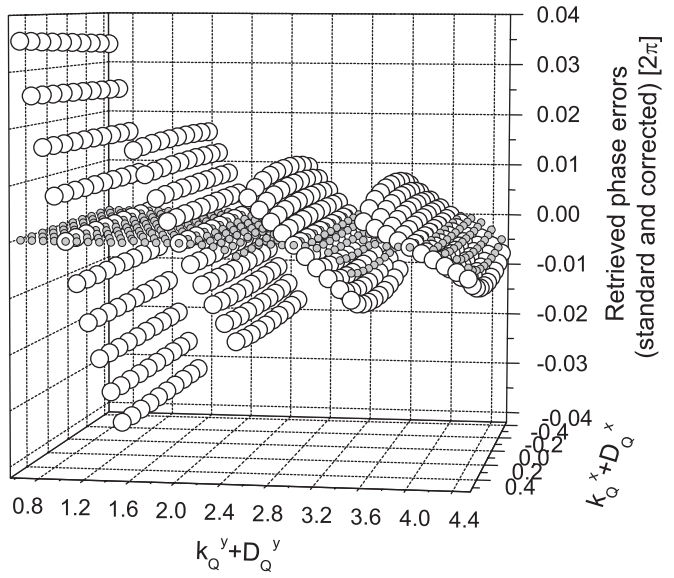

Fig. 3. Difference between the retrieved phase and the initially set phase, in units of 2π, as a function of integer and non-integer parts of spatial carrier frequency components, shown in a small part of Fourier space. Larger open circles show the retrieved phase error obtained using standard Eq. (6), and small grey circles show the retrieved phase error reduced by using Eq. (12). Parameters are: $N = M = 64$, $\bar{b}/\bar{a} = 0.5$, $\phi_{\text{in}} = 0.155$, $\alpha = 3$.

sidelobes of the product of two SINC functions depending on k^x and k^y falls off roughly as k^{-2} in Fourier space, but only as k^{-1} along the horizontal or vertical direction). The magnitude of the errors is clearly suppressed several times by using the corrected expression, especially for the low as well as high density of fringes within the image field. The error is almost negligible in the intermediate region, even using the standard Eq. (6), but is nevertheless reduced by applying Eq. (12). (The enlarged view insets show the interval of k_Q^x values where the error is smaller than ± 0.35 nm for horizontal fringes, and another order of magnitude smaller for diagonal fringes, $k_Q^x = k_Q^y$. In our case the growth of a single atom layer on the (1 1 1) facet of $Cu_{2-x}Se$ is equivalent to displacement of 0.35 nm.) As these parameters (density and orientation of fringes) can be adjusted by fine tuning the elements of the experimental set-up, these results can be considered as guidelines for performing more reliable and accurate measurements—by choosing the working parameters' values within the range, which we have clearly defined, where the intrinsic error is acceptably small and/or by applying the hereby described modified algorithm for reducing it (enjoying the additional benefit of remaining all the time within the experimentally comfortable 2D situation).

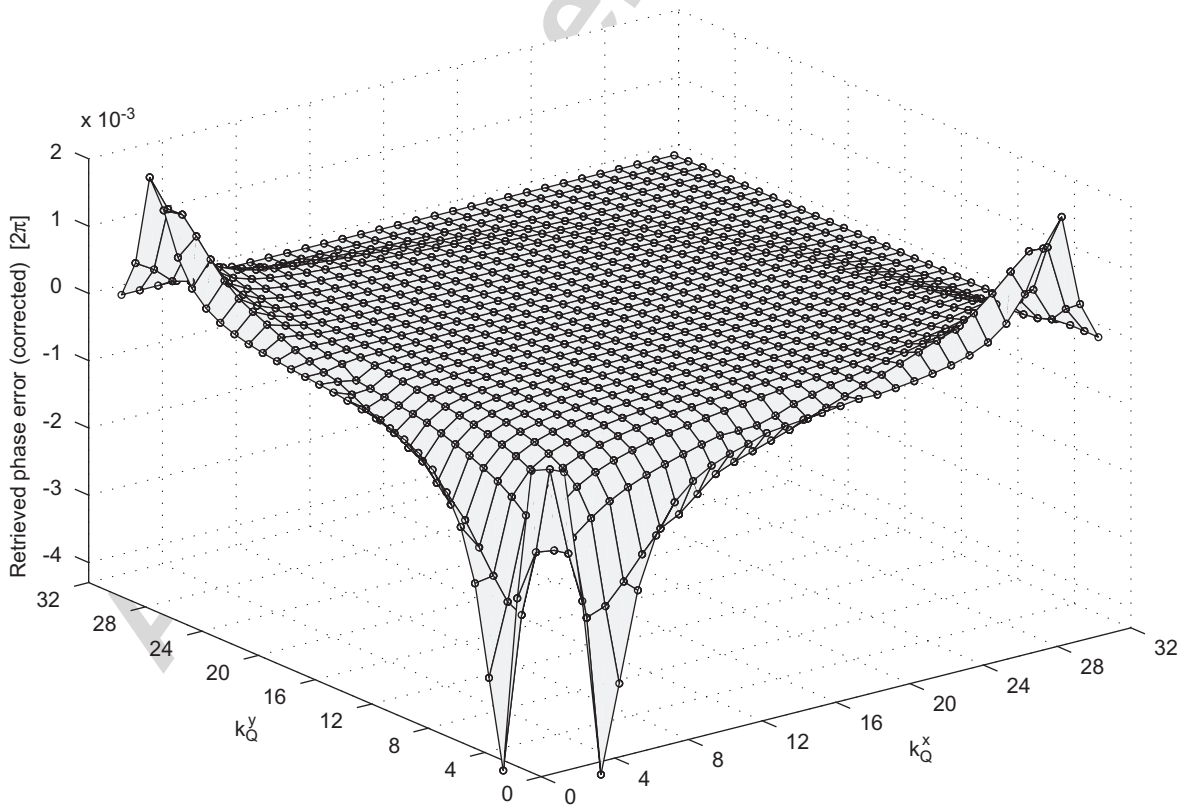

Fig. 4. Difference between the retrieved phase (from Eq. (12)) and the initially set phase, in units of 2π, as a function of integer spatial frequency components k_Q^x and k_Q^y (compare with Fig. 2; note that the vertical scale here is smaller by an order of magnitude). Parameters are: $N = M = 64$, $\bar{b}/\bar{a} = 0.5$, $\phi_{\text{in}} = 0.155$, $\alpha = 3$, $D_Q^x = 0.5$ and $D_Q^y = 0.5$.

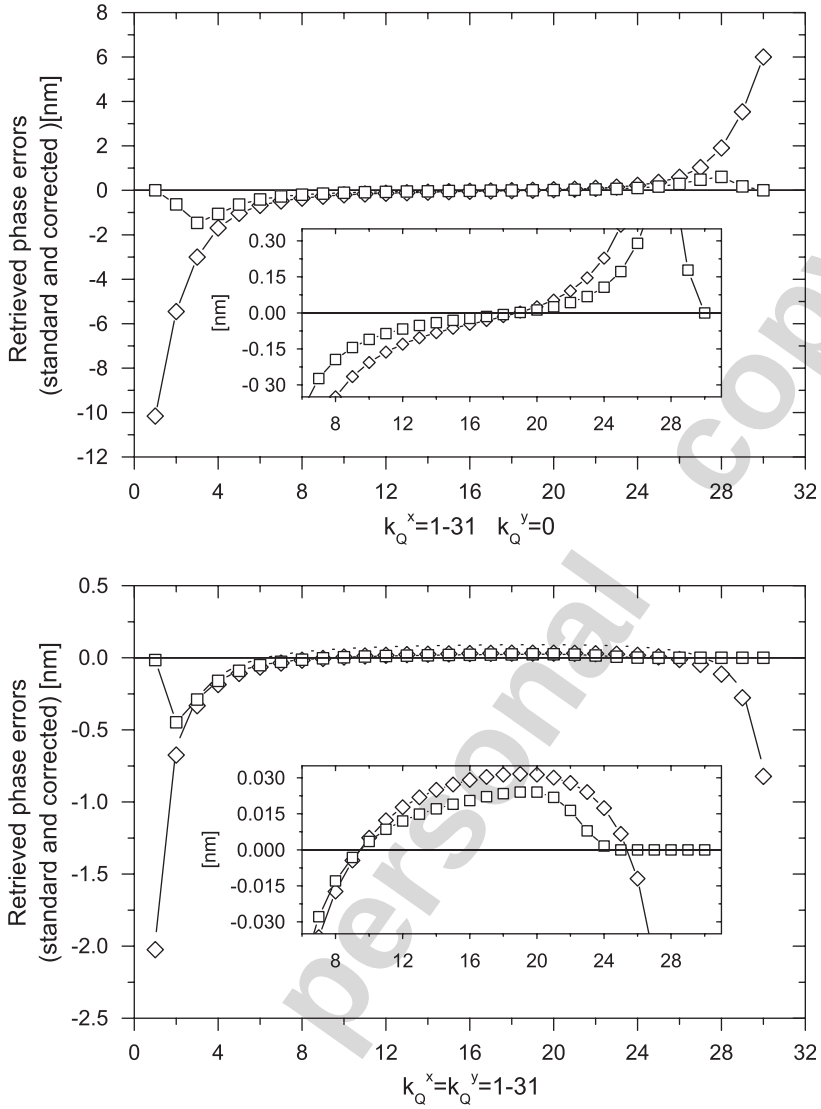

Fig. 5. Comparison of the retrieved phase errors (given in nanometres as the corresponding displacement of the observed object) using standard ($\diamond$, Eq. (6)) and corrected ($\square$, Eq. (12)) expressions. The upper panel is for interferometric fringes parallel to the x-axis, and the lower panel for fringes running diagonally. The insets show enlarged view of parameter range within which the errors are practically negligible. Parameters are: $N = M = 64$, $\bar{b}/\bar{a} = 0.5$, $\phi_{\text{in}} = 0.155$, $\alpha = 3$, $D_Q^x = 0.5$ and $D_Q^y = 0.5$.

5. Conclusions

Striving to measure as precisely as possible the values of radial displacements of facets on the surface of growing spherical single crystals of $Cu_{2-\delta}Se$ using digital laser interferometry method, we have undertaken to test the reliability and accuracy of standard Fourier analysis procedure for phase retrieval from interference fringe patterns. We have studied the realistic, quite general 2D case of digitally recorded interferograms, investigating a wide range of experimentally accessible, adjustable parameters (fringe density and orientation) on a model interferogram. We demonstrated the existence of inherent errors in the retrieved phase due exclusively to the non-integer number of interferometric fringes within the observed digitally sampled image obtained from a CCD camera. Within the framework of the usual procedure (Fourier fringe analysis) for retrieving the phase value, we introduced fully adjustable custom designed 2D Gaussian filtering window. The appropriate 2D unwrapping of the retrieved phase field is applied as consecutive multiple-stage unwrapping algorithm. The obtained phase field must be averaged over the entire selected interferogram area. Comparing the retrieved phase with the initially set one, we showed the dependence of the retrieved phase errors on the input phase value, fringe density and orientation (for generally non-integer 2D modulation wave vector). We presented a modified expression to replace the one usually used for phase retrieval, which results in a significant reduction of the error amplitude, particularly for low as well as high fringe density values. Our results show that there is a range of experimentally selectable parameters

within which the retrieved phase error, expressed as the observed equivalent facet displacement, is smaller than ± 0.35 nm in the case of interferometric fringes running parallel to x- or y-axis of the interferogram (equivalent to 1D projection case), but even smaller than ± 0.035 nm in the case of diagonally oriented fringes within 2D image field.

Acknowledgements

We acknowledge gratefully the financial support of the Ministry of Science, Education and Sport of the Republic of Croatia.

References

[1] Ohachi T, Taniguchi I. Growth of α-Ag_2S and α-Ag_2Se single crystal through a capillary tube. In: Vashishta P, Mundy JN, Shenoy GK, editors. Fast ion transport in solids, electrodes and electrolytes. New York, Amsterdam, Oxford: North Holland; 1979. p. 597–600.

[2] Ohachi T, Taniguchi I. Roughening transition for the ionic–electronic mixed superionic conductor α-Ag_2S. J Cryst Growth 1983;65:84–8.

[3] Ohachi T, Imai S, Tanaka T, Yamai H, Taniguchi I. Semiconducting and atomic properties of the mixed conductor α-Ag_2S. Solid State Ion 1988;28–30:1160–6.

[4] Vučić Z, Gladić J. Shape relaxation during equilibrium—like growth of spherical cuprous selenide single crystals. Fizika A (Zagreb) 2000;9(1):9–26 〈http://fizika.phy.hr/fizika_a/av00/a9p009.htm〉.

[5] Vučić Z, Gladić J. Growth rate of equilibrium-like-shaped single crystals of superionic conductor cuprous selenide. J Cryst Growth 1999;205:136–52.

[6] Gladić J, Vučić Z, Lovrić D. Critical behaviour of the curved region near 111–facet edge of equilibrium shape cuprous selenide large single crystals. J Cryst Growth 2002;242:517–32.

[7] Ruutu JP, Hakonen PJ, Babkin AV, Parshin ZuA, Tvalashvili G. Growth of ^{4}He crystals at mK temperatures. J Low Temp Phys 1998; 112:117–64.

[8] Lovrić D, Vučić Z, Gladić J, Demoli N, Mitrović S, Milas M. Refined Fourier-transform method of analysis of full 2D digitized interferograms. Appl Opt 2003;42(8):1477–84.

[9] Kostianovski S, Lipson SG, Ribak EN. Interference microscopy and Fourier fringe analysis applied to measuring spatial refractive–index distribution. Appl Opt 1993;32(25):4744–55.

[10] Takeda M, Ina H, Kobayashi S. Fourier-transform method of fringe-pattern analysis for computer-based topography and interferometry. J Opt Soc Am 1982;72(1):156–60.

[11] Vučić Z, Gladić J. Phase retrieval errors in standard Fourier fringe analysis of digitally sampled model interferograms. Appl Opt 2005;44:6940–7.

[12] Press WH, Teukolsky SA, Vetterling WT, Flannery BP. Numerical recipes in Fortran. 2nd ed. Cambridge: Cambridge University Press; 1992. p. 542–51.

[13] Kattoush Abbas. A new recurrent approach for phase unwrapping. Int J Appl Sci Eng 2005;3(2):135–43.